Developmental Biology 421 (2017) 8–15

Contents lists available at ScienceDirect

Developmental Biology

journal homepage: www.elsevier.com/locate/developmentalbiology

Short Communication

The Sec domain protein Scfd1 facilitates trafficking of ECM components during chondrogenesis

Ningning Hou[a], Yuxi Yang[a], Ian C. Scott[b,c], Xin Lou[a,*]

[a] Model Animal Research Center, Nanjing University, China
[b] Program in Developmental and Stem Cell Biology, The Hospital for Sick Children, Canada
[c] Department of Molecular Genetics, University of Toronto, Canada

ARTICLE INFO

Keywords:
scfd1
Chondrogenesis
Collagen
Intracellular transport
Zebrafish
Craniofacial development

ABSTRACT

Chondrogenesis in the developing skeleton requires transformation of chondrocytes from a simple mesenchymal condensation to cells with a highly enriched extracellular matrix (ECM). This transition is in part accomplished by alterations in the chondrocyte protein transport machinery to cope with both the increased amount and large size of ECM components. In a zebrafish mutagenesis screen to identify genes essential for cartilage development, we uncovered a mutant that disrupts the gene encoding Sec1 family domain containing 1 (*scfd1*). Homozygous *scfd1* mutant embryos exhibit a profound craniofacial abnormality caused by a failure of chondrogenesis. Loss of *scfd1* was found to hinder ER to Golgi transport of ECM proteins and is accompanied with activation of the unfolded protein response in chondrocytes. We further demonstrate a conserved role for Scfd1 in differentiation of mammalian chondrocytes, in which loss of either SCFD1 or STX18, a SLY1 interacting t-SNARE, severely impair transport of type II collagen. These results show that the existence of a specific export pathway, mediated by a complex containing SCFD1 and STX18 that plays an essential role in secretion of large ECM proteins during chondrogenesis.

1. Introduction

Cartilage formation and skeletal morphogenesis depend on timely and abundant deposition of extracellular matrix (ECM) proteins (DeLise et al., 2000; Zuscik et al., 2008). The major ECM component of cartilage is type II collagen, which constitutes up to 60% of the total cartilage protein content (Mow et al., 1992; Sophia Fox et al., 2009). The synthesis and secretion of collagens and other ECM proteins are precisely and dynamically regulated as chondrogenesis proceeds. Failure to produce adequate mature collagen fibers leads to developmental defects and diseases such as osteogenesis imperfecta (Bateman et al., 2009; Rauch and Glorieux, 2004). Transport of ECM proteins to the extracellular space is dependent on the secretory machinery. Trafficking of ECM proteins is initiated as they leave their site of synthesis in the endoplasmic reticulum (ER) and are transported to the Golgi apparatus. Fibrillar collagen forms as a rigid rod-like triple helix with a length over 300 nm (Lamande and Bateman, 1999), presumably too large to fit into canonical COPII-coated transport vesicles, which are typically 60–80 nm in diameter. This strongly suggests that a distinct vesicular transport mechanism exists through which cartilage-specific collagens are actively packaged, likely requiring specific cargo receptors and/or chaperones.

SCFD1 (also known as SLY1) is a member of the Sec1/Munc18 family of proteins that cooperate with SNARE complexes in membrane fusion events (Carr and Rizo, 2010). The yeast ortholog of SCFD1 has been implicated in forward and retrograde trafficking to the ER (Li et al., 2005) and quality control of membrane fusion (Lobingier et al., 2014). In mammalian cells, several functions have been shown for SCFD1. SCFD1, in conjunction with Syntaxin 5, has been reported to be involved in ER to Golgi transport *via* assembly of pre-Golgi intermediates through interactions with Syntaxin 17 and 18 (Dascher and Balch, 1996; Rowe et al., 1998; Steegmaier et al., 2000; Yamaguchi et al., 2002). SCFD1 has also been suggested to play a role in intra-Golgi and retrograde transport *via* association with the COG4 complex (Laufman et al., 2009). Recently, Nogueira et al. reported that SCFD1 binds to TANGO1 and specifically regulates Procollagen VII export (Nogueira et al., 2014). While informative, these proposed roles of SLY1 in protein transport were primarily intuited based on the use of artificial cargoes such as a temperature-sensitive Glycoprotein mutant of the Vesicular Stomatitis Virus. The endogenous cargoes of SLY1-associated vesicles and the molecular mechanism underlying the transport of these vesicles is therefore a matter of debate. In previous

* Correspondence to: Model Animal Research Center, Nanjing University, Rm 403B, 12 Xuefu Road, Nanjing, Jiangsu, China.
E-mail address: xin.lou@nju.edu.cn (X. Lou).

http://dx.doi.org/10.1016/j.ydbio.2016.11.010
Received 4 May 2016; Received in revised form 12 October 2016; Accepted 13 November 2016
Available online 13 November 2016
0012-1606/

work, a temperature sensitive zebrafish *scfd1* mutant was used to demonstrate a requirement for SCFD1 in regenerative outgrowth of the fin (Nechiporuk et al., 2003). However, due to the hypomorphic nature of this mutant allele, the *in vivo* function of SCFD1 was not fully addressed, particularly during embryogenesis.

In this current study, we present data on the identification and characterization of a zebrafish *scfd1* null mutant recovered from a gene trapping screen. We show that *scfd1* is essential for extracellular matrix secretion in cartilage. *Scfd1* mutants exhibit a failure in chondroblast differentiation and induce a strong unfolded protein response (UPR) in chondrocytes. We further demonstrate that SCFD1 and STX18, a SCFD1 interacting t-SNARE, are necessary for Procollagen II transport in a mammalian chondrocyte differentiation model. These data provide mechanistic insights into the central role of SCFD1 within the chondroblast to facilitate the formation of large ER transport vesicles involved in the exportation of cartilage collagens and, perhaps, collagen-associated molecules of the ECM. Our results further suggest that mutations affecting SCFD1 and other proteins mediating collagen export are potential causes for congenital craniofacial abnormalities and skeletal diseases of unknown genetic origin.

2. Materials and methods

2.1. Zebrafish lines

Zebrafish embryos were maintained and staged using standard techniques (Westerfield, 1993). *Tg(sox10:EGFP)^{ir937}* fish has been previously described (Piloto and Schilling, 2010). The RP-T gene trap vector was modified from RP2 and co-injected with Tol2 transposase mRNA as previously described (Clark et al., 2011). To identify the affected gene in the gene trap lines, 5' RACE was carried out as previously described (Clark et al., 2011). The *hsp70:scfd1*; *α-crystallin:EGFP* transgenic line was generated by using standard Tol2 transgenesis (Kawakami, 2005). Full-length zebrafish *scfd1* coding sequence was subcloned downstream of a *hsp70* promoter in a backbone vector carrying a α-*crystallin:EGFP* marker cassette (Burrows et al., 2015). Heat shock was performed for 30 min in pre-warmed 37 °C media.

2.2. Alcian blue staining, immunohistochemistry and WGA staining

Alcian blue staining (Walker and Kimmel, 2007), immunohistochemistry and WGA staining (Sarmah et al., 2010) were performed as previously described. Primary antibody specific to Collagen II (II-II6B3, obtained from DHSB, 1:200 dilution) was used. Fluorescent immunocytochemistry was performed using anti-mouse antibody conjugated with Cy3 (1:1000 dilution, Sigma) and WGA–Alexa-Fluor-488 conjugate (1:200 dilution, Life Technology).

2.3. Imaging

Imaging was performed using a Leica DFC320 camera on a Leica M205FA stereomicroscope. All confocal images were taken on a Zeiss LSM510 confocal microscope.

2.4. *RNA* in situ *hybridization*

Transcription of DIG-labeled antisense RNA probes was performed using standard methods. RNA *in situ* hybridization (ISH) was carried out as previously described (Thisse and Thisse, 2008).

2.5. Cell death assay

Cell death assays were performed as previously described (Caron et al., 2008; Verduzco and Amatruda, 2011) using a Cell Death Assay Detection Kit, POD (Roche).

2.6. Quantitative real-time PCR

Total RNA was prepared using TRIzol (Invitrogen, Life Technologies Corp.) from 50 combined control or *scfd1* mutant embryos, with mutants being identified morphologically. Control larvae were phenotypically wild type sibling embryos (mixture of nullizygous and hemizygous for the gene trap allele). Primers used for qPCR analysis are listed in Table S1.

2.7. Electron microscopy

After being anesthetized with tricaine (Sigma), zebrafish embryos were placed into fresh 4% paraformaldehyde and incubated overnight at 4 °C. Sample processing, sectioning and imaging were carried out as previous described (Melville et al., 2011).

2.8. Western blotting

Proteins were isolated by homogenizing 3 dpf embryos in RIPA buffer containing protease inhibitor (Sigma). Procedures of western blotting and antibodies were described in Supplementary Experimental Procedures.

2.9. Cell culture and Alcian blue staining of ATDC5 cells

Culture, insulin stimulation and Alcian blue staining of ATDC5 cells were carried out as previously described (Yang et al., 2009).

2.10. Establishment of knockdown stable cell lines

The mammalian pSUPER-puro vectors were used for expression of short hairpin (sh) RNAs corresponding to mouse cDNAs (target sequences listed in Table S2). ATDC5 cells were transfected with the Sly1, TANGO or Syntaxin 18 shRNA constructs, and 36 h later were transferred into selection medium containing 0.5 mg/ml puromycin. Depletion of gene expression in puromycin-resistant clones was verified by western blotting. A stable cell line harboring an empty pSUPER vector was established and used as a control.

2.11. Flow cytometric analysis of apoptosis

Membrane and nuclear events during apoptosis were analyzed by flow cytometry using FITC-Annexin V and propidium iodide (PI) staining and an Alexa Fluor® 488 Annexin V/Dead Cell Apoptosis Kit (ThermoFisher).

3. Results and discussion

3.1. Loss of scfd1 leads to defects in craniofacial chondrogenesis

In a *Tol2* transposon-mediated gene trapping screen to identify novel genes essential for embryogenesis (Fig. 1A), we identified a line, RT-104B, showing chondrocyte specific GFP expression from 60 h post-fertilization (hpf) until 7 day post-fertilization (dpf) (data not shown and Fig. 1B–L). GFP expression also could be observed in gastrointestinal organs, brain, ovary and fin in larvae and adult fish (Fig. S1). This dynamic expression pattern suggested a role for the trapped gene in development and physiological function of multiple organs. Homozygous mutant embryos from incrosses of heterozygous RT-104B fish showed no obvious morphological defects until 48 hpf (Fig. 2A and B), and died by 7 dpf. By 72 hpf, RT-104B homozygous mutant embryos had a reduced lower jaw, with no cartilage formation evident by Alcian blue staining (Fig. 2C and D and data not shown). At 96 hpf, only posterior portions of trabeculae and residual parachordal plate were formed in mutant embryos, whereas the viscerocranium (lower jaw) was completely absent (Fig. 2G–I). In addition to defects in

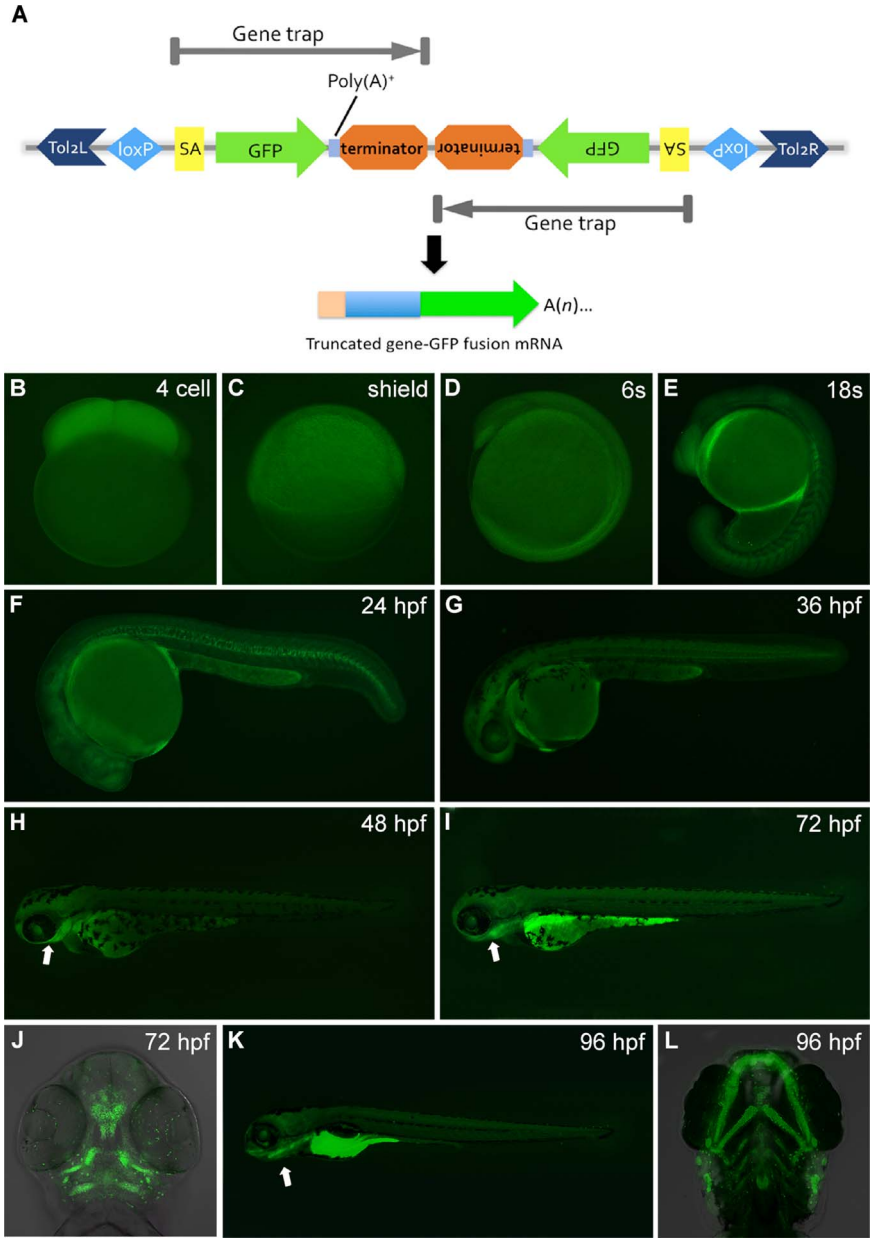

Fig. 1. Gene trapping construct and GFP expression pattern of gene trap line RP24-104 during embryogenesis. (A) Schematic of RP-T gene trapping construct. RP-T transposon system composed of two protein-trap cassettes with a transcriptional stop in the opposite direction. Tol2L and Tol2R, tol2 transposase inverted terminal repeat; SA, splice acceptor; GFP, AUG-less monomeric GFP sequence; poly(A)+, polyadenylation signal; terminator, transcriptional border element. (B–L) GFP expression pattern in zebrafish gene trap line RP24-104. Prior to 16-somite stage, GFP signal could be observed in the whole embryo (B to D). From 16-somite stage, elevated signal could be observed in notochord on the ubiquitous GFP expression background (E). As development proceeded, the GFP signal was gradually constrained to the pharyngeal region and cartilage tissue (H, I, J, K and L). From 96 hpf, apparent signal could be observed in the gastrointestinal organs (K) and serotonergic neuroepithelial cells on the skin (L). B and C, lateral view with animal pole to the top. D and E, lateral view with anterior to the top. F-I and K, lateral views with head to left. J and L, ventral views with anterior to the top.

cartilaginous tissue, Alcian blue staining also revealed the absence of goblet cells in the intestine of RT-104B homozygous mutant embryos (Fig. S2), which suggested the trapped gene is involved in the differentiation of goblet cells.

In order to identify the causative mutation in the RT-104B line, 5' RACE was carried out. Sequencing indicated that the gene trapping element was integrated within the 1st intron of the *scfd1* locus (Fig. 2J). Consistent with the gene trapping event, endogenous *scfd1* expression closely matched that of the GFP expression pattern in RT-104B embryos, including prominent transcript localization in the pharyngeal region from 48 to 96 hpf (Fig. S3A–G). Maternal expression of *scfd1* was evident (Fig. S3A) and maternally deposited Scfd1 protein persisting in mutant embryos until 24 hpf (Fig. S4), which could explain relatively normal development at earlier stages. The zebrafish Scfd1 protein contains a conserved Sec1-like domain spanning amino acids 143–273. The gene trap insertion resulted in a fusion transcript that encoded a protein containing only the first N-terminal 10 amino acids of SCFD1 (Fig. 2K). Q-PCR and western blotting demonstrated no detectable full-length *scfd1* transcript or protein in RT-104B homozygous embryos from 48 hpf onwards (Fig. 2L and M). To further confirm whether the phenotype in RT-104B line was induced by loss of *scfd1*, we generated a transgenic line expressing WT *scfd1* mRNA under control of an inducible *hsp70* promoter. Broad *scfd1* expression had no apparent effects on development (data not shown). Re-introduction of wildtype Scfd1 by heat shock starting at 24 hpf resulted in rescue of the cartilage defects in RT-104B homozygous embryos (Fig. 2N and O). These results indicated that the RT-104B gene trap phenotype is due to an *scfd1* null (full loss-of-function)

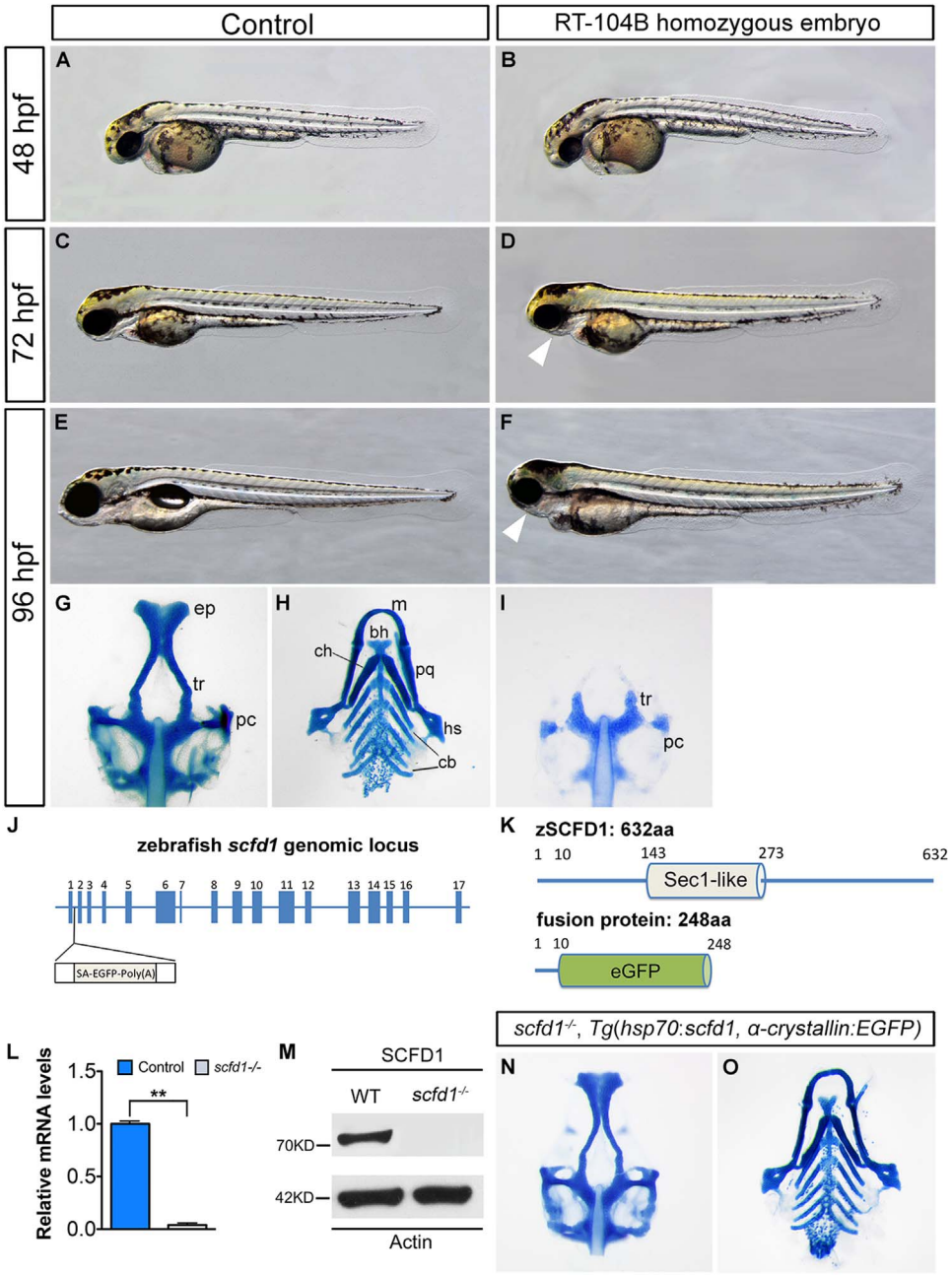

Fig. 2. Loss of *scfd1* disrupts craniofacial skeletal development. (A–F) Live images of wild type (control) and RP24-104B homozygous embryos at indicated developmental stages. Lateral view with head to left. (G–I, N and O) Alcian blue staining of cartilage elements in head skeleton in ventral views. White arrowheads indicate dismorphic jaw. bh, basihyal; cb, ceratobranchial; ch, ceratohyal; ep, ethmoid plate; hs, hyosymplectic; m, Meckel's cartilage; pc, parachordal plate; pq, palatoquadrate; tr, trabeculae. (J) The zebrafish *scfd1* genomic locus. The transposon is inserted after the first exon. (K) Schematic representations of the domain structure of the wild type zebrafish SCFD1 protein and fusion protein in the gene trap *scfd1* mutant. (L and M) Q-PCR and western blotting experiments confirmed loss of *scfd1* expression in homozygous mutant embryos at 48 hpf. **P < 0.01 as determined by Student's *t*-tests. Error bars indicate s.e.m. (N and O) Rescue of the *scfd1* mutant phenotype in *Tg(hsp70:scfd1; α-crystallin:EGFP)* embryos at 96 hpf. Heat shock was performed every 12 h from 24 hpf onwards.

mutation.

3.2. ECM protein trafficking is disrupted in scfd1 mutant chondrocytes

We next sought to uncover the mechanism of Scfd1 function in chondrogenesis. Examination of expression of markers of pre-migratory neural crest (*sox9b*, *foxd3* and *snail1b*), migratory facial neural crest (*dlx2a* and *twist1a*), pharyngeal arch patterning and outgrowth (*hand2*, *dlx2b* and *dlx3b*) and regulators of mesenchymal condensation formation (*goosecoid* and *sox9a*) revealed no apparent defects in *scfd1* mutants from 14 to 72 hpf (Fig. S5A–K; Minoux and Rijli, 2010; Sasaki et al., 2013; Stuhlmiller and Garcia-Castro, 2012; Yan et al., 2002; Zuscik et al., 2008). The differentiation of chondroprogenitors is characterized by the deposition of a cartilage matrix, which contains Collagen II as the primary component (Goldring et al., 2006). RNA *in situ* hybridization revealed slightly reduced *col2a1a* expression at 72 hpf in *scfd1* mutant embryos, with a greater reduction in expression in the developing jaw at 96 hpf (Fig. 3A–D) (the mis-expression of collagen could be caused by ER stress, see further discussion of this in Section 3.3).

To directly examine ECM components, histological sections of 84 hpf embryos were stained with toluidine blue, which stains cartilage proteoglycans (Melville et al., 2011). A large reduction in the extent of

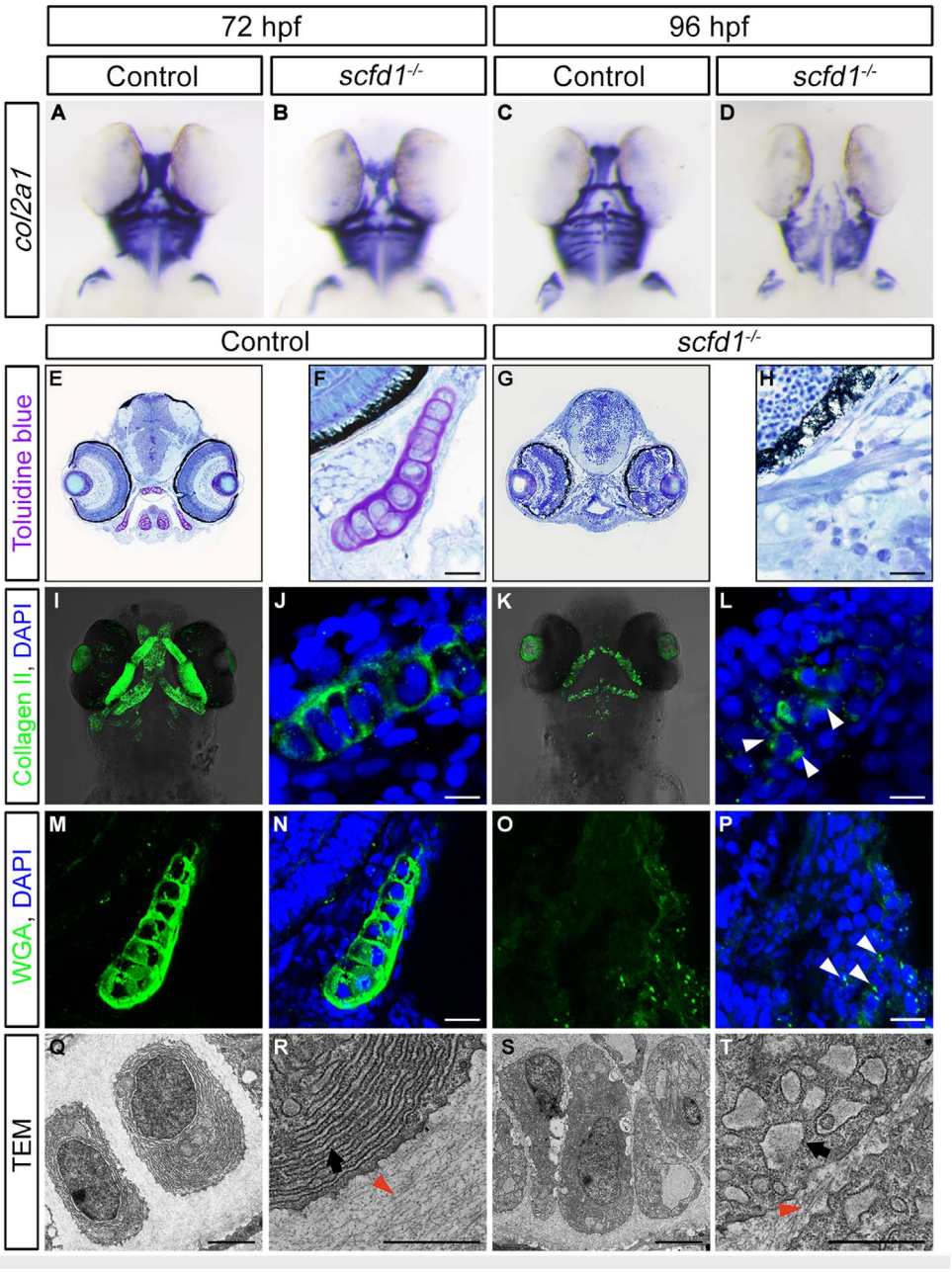

Fig. 3. Protein trafficking is disrupted in *scfd1* mutants. (A–D) Chondrocytes in *scfd1* mutant embryo express *col2a1a* normally at 72 hpf, with reduced expression by 96 hpf. A to D, ventral views with anterior to the top. (E-H) Toluidine blue staining of transverse sections of the jaw at 80 hpf. Nuclei are stained blue, whereas ECM is stained purple. (I–P) Immunostaining of Collagen II and WGA in the palatoquadrate of 80 hpf wild type and *scfd1* mutant embryos. Arrowheads in L and P indicate aberrant intracellular ECM protein localization in a *scfd1* mutant. (Q–T) TEM images of 80 hpf wild type and *scfd1* mutant chondrocytes. Black arrows indicate well-stacked ER in wild type cell (R) or distended ER membranes in *scfd1* mutant cells (T). Orange arrowheads point to collagen fibril deposition in the extracellular space. Scale bars: 25 μm (F, H, J, L, N and P); 2 μm (Q–T). For A to P, at least 15 embryos for each genotype were analyzed and representative samples are shown. For Q to T, 6 embryos for each genotype were analyzed and representative samples are shown.

ECM surrounding chondrocytes in *scfd1* mutants was evident (Fig. 3E–H). In addition to abnormal chondrogenic ECM, mis-organized cells in the retina could also be observed (Fig. 3, compare E and G), which indicated a role for *scfd1* in eye development. We next examined at 80 hpf the cellular distribution of Collagen2a1 (Collagen II) by immunostaining and bulk secreted glycoproteins by staining with wheat germ agglutinin (WGA). In wild type embryos, both Collagen II and WGA signals were primarily localized to the extracellular space surrounding chondrocytes. In contrast, accumulation of Collagen II and glycoproteins in cytosolic vesicle-like structures was evident in *scfd1* mutants (Fig. 3I–P). Transmission electron microscopy (TEM) was used to more closely examine intracellular protein buildup in *scfd1* mutants. TEM images revealed that while in wild type embryos cuboidal chondrocytes were stacked in a regular fashion and separated from each other by dense ECM, in *scfd1* mutant embryos chondrocytes had an irregular morphology, surrounded by a sparse ECM and were often attached to each other (Fig. 3Q and S). In wild type chondrocytes, rough ER (ribosome dotted membranes) was well developed and organized. Conversely, *scfd1* mutant chondrocytes contained large vacuoles of severely distended ER membranes filled with electron dense material (Fig. 3R and T).

These results suggested a key role for *scfd1* in extracellular transport of ECM components in chondrocytes. In order to directly confirm the cellular autonomy of *scfd1* function, we employed a transplantation approach (Fig. S6E). Using *sox10:EGFP* donor embryos, in which EGFP is expressed in neural crest-derived chondrocytes

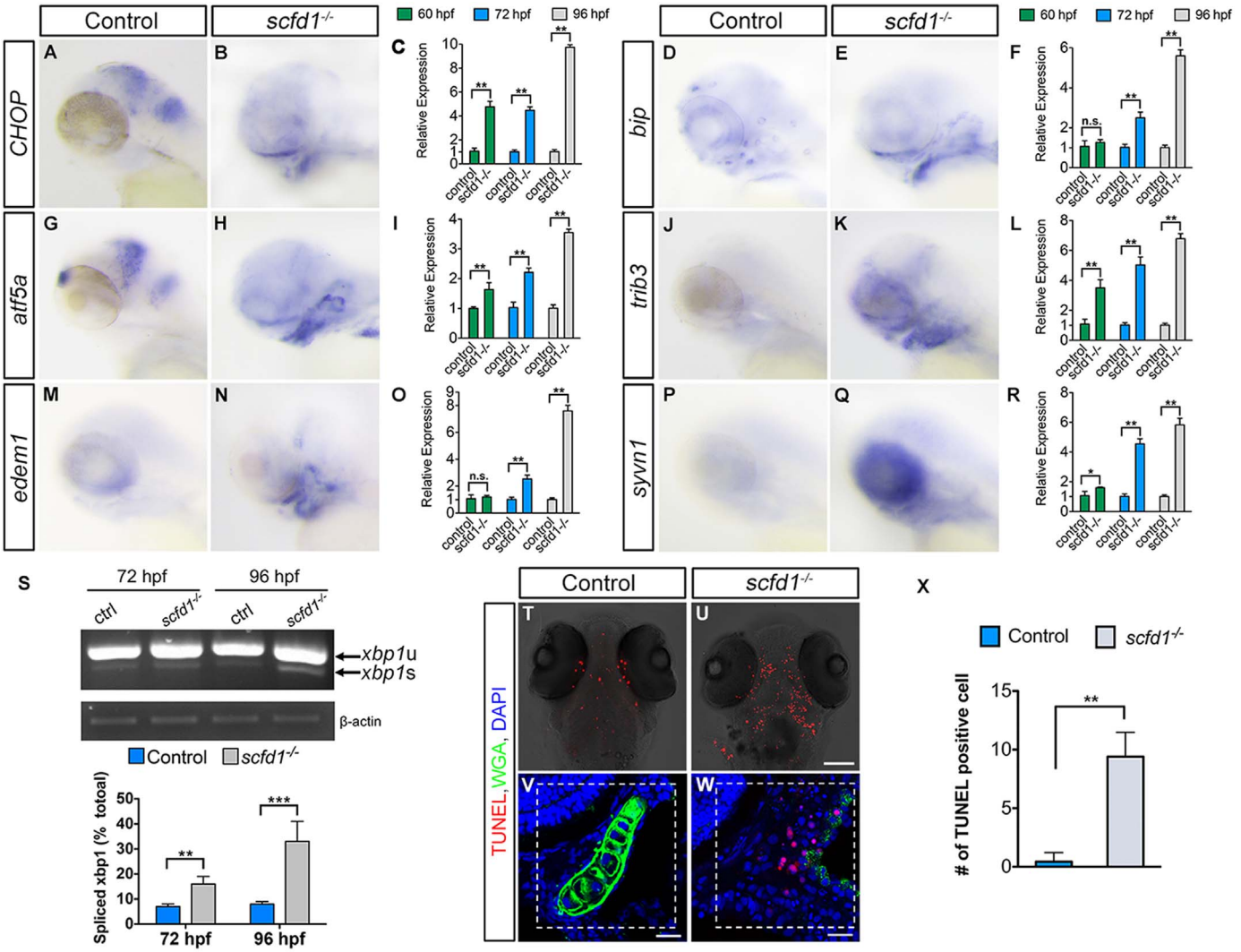

Fig. 4. The UPR is activated in *scfd1* mutant embryos coincident with up-regulated cell death. (A, B, D, E, G, H, J, K, M, N, P and Q) Whole mount *in situ* hybridization of 72 hpf wild type and *scfd1 mutant* embryos using probes against *ditt3, hspa5, atf5, trib3, edem1* and *syvn1*. Lateral views with anterior to the left. (C, F, I, L, O and R) Q-PCR experiments confirmed up-regulation of UPR-associated genes in *scfd1* mutants. Error bars represent mean ± SEM. (S) Elevated *xbp1* mRNA splicing was detected by RT-PCR and Q-PCR. *xbp1*-u, unspliced *xbp1* mRNA. *xbp1*-s, spliced *xbp1* mRNA. β-actin was as a loading control for RT PCR. Percentage of spliced *xbp1* mRNA determined by the percentage of spliced/total mRNA. Error bars indicate s.e.m. n.s., not significant. $^{**}P < 0.01$ and $^{*}P < 0.05$ as determined by Student's *t*-tests (C, F, I, L, O and R). (T–X) Enhanced cell death in scfd*1* mutants. Ventral view with anterior to the top. (V, W and X) Quantification of TUNEL-positive cells counted on a 0.016 mm^2 field (dashed line square). 8 sections for each genotype were analyzed and representative samples are shown. Error bars indicate s.e.m. $^{**}P < 0.01$ as determined by Student's *t*-tests. Scale bars: 25 μm.

(Fig. S6A–D), we found that at 96 hpf wild type *sox10:EGFP* donor cells could contribute to the jaw cartilage in both wild type (43% of transplants, n=41) and *scfd1* mutant (36% of transplants, n=37) host backgrounds (Fig. S6F–I and N–P). In contrast, when *scfd1* mutant *sox10:EGFP* donor cells were used, no contribution to cartilage was observed (Fig. S6J–M, n=31), although donor cells persisted in the head based on expression of a rhodamine lineage tracer. Using Alcian blue staining, we further found that in *scfd1* mutant host embryos wild type donor cells could partially restore the anterior neurocranium (Fig. S6Q–T, 31% of transplants, n=22). This indicated that *scfd1* is required cell autonomously, in chondrocytes, for proper cartilage development.

3.3. Loss of scfd1 triggers an ER stress response in chondrocytes

Given the distended ER revealed by TEM and intracellular aggregates of ECM proteins detected by immunostaining in *scfd1* mutant chondrocytes, we hypothesized that stresses in mutant chondrocytes may result in activation of the unfolded protein response (UPR) and the induction of ER associated protein degradation (ERAD). Expression analysis of the primary UPR driver *ditt3* and targets of the atf4-ditt3 pathway, *hspa5*, *atf5a* and *trib3* (Hetz, 2012; Wang and Kaufman, 2014), by RNA *in situ* hybridization revealed specific up-regulation of the UPR throughout the pharyngeal region of *scfd1* mutant embryos (Fig. 4A–L). Gene expression profiling by Q-PCR of 60, 72, and 96 hpf embryos confirmed a highly significant increase in expression of genes associated with the UPR. Mediators of ERAD, such as *edem1* and *syvn1*, were also highly up-regulated in *scfd1* mutants (Fig. 4M–R). To further confirm the activation of IRE1-XBP1 branch of the UPR, the splicing of *xbp1* mRNA was assayed by RT-PCR and Q-PCR. Both experiments showed significant enhanced *xbp1* splicing in *scfd1* mutant (Fig. 4S). If accumulation of misfolded proteins in the ER is not resolved, prolonged UPR will both inhibit proliferation and induce programmed cell death, thus helping cells or tissues to cope with the consequences of ER stress (Fribley et al., 2009; Vandewynckel et al., 2013). We therefore next analyzed apoptosis in *scfd1* mutants. Whole-mount TUNEL staining revealed that at 72 hpf an increased incidence of apoptosis was evident in the pharyngeal region of *scfd1* mutant embryos (Fig. 4T–X). These data indicated that the UPR was triggered in *scfd1* mutants, with apoptosis induced by the UPR

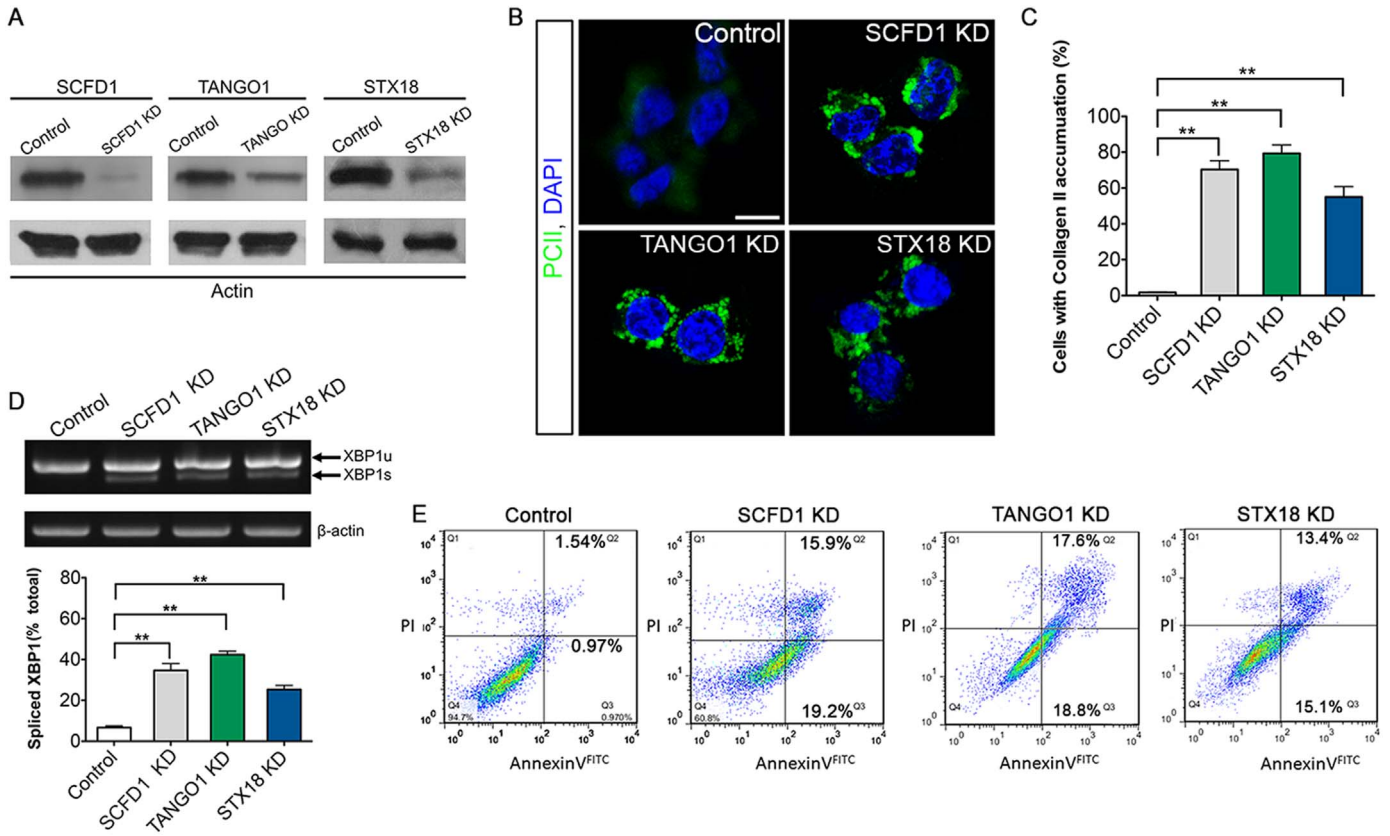

Fig. 5. SCFD1 and STX18 are necessary for Procollagen II transport. (A) Efficiency of knockdown of SCFD1, TANGO1 and STX18 as measured by western blotting. (B) Quantification of cells that accumulate Procollagen II intracellularly. The percentage of cells that accumulate Procollagen II intracellularly was determined by counting at least 30 cells in five random fields. The number of cells accumulating Procollagen II in the case of SCFD1, TANGO1 and STX18 shRNA was significantly elevated as compared to control shRNA cells. Error bars indicate s.e.m. $^{**}P < 0.01$ as determined by Student's *t*-tests. (C) ATDC5 cells were visualized with anti-Collagen II antibody and DAPI. Scale bar, 20 μm. (D) Elevated XBP1 mRNA splicing in ATCD5 cell was detected by RT-PCR and Q-PCR. XBP1-u, unspliced XBP1 mRNA. XBP1-s, spliced XBP1 mRNA. β-actin served as a loading control. Error bars represent mean ± SEM. $^{**}P < 0.01$ as determined by Student's *t*-tests. (E) Apoptosis in ATDC5 cells detected by FACS analysis. The right quadrants (Q2 and Q3) represent apoptotic cells, with cytoplasmic membrane integrity. The average apoptotic rates of control, SCFD1 knockdown, TANGO1 knockdown and STX18 knockdown samples were 2.51 ± 0.56, 35.11 ± 0.40, 36.43 ± 1.31 and 28.58 ± 2.32%, respectively.

potentially contributing to the craniofacial phenotype.

3.4. *Scfd1 and Syntaxin18 are necessary for Procollagen II transport*

SCFD1 can bind to TANGO1 at ER exit sites, and co-operates with STX18, a SCFD1 interacting tSNARE, to specify a distinct export pathway for Procollagen VII (Nogueira et al., 2014). We next sought to determine if the functions we described for zebrafish Scfd1 were more generally applicable to vertebrate chondrogenesis. To this end we tested the function of SCFD1 and STX18 in Collagen II transportation in an *in vitro* mammalian chondrocyte differentiation system. Mouse ATDC5 chondroprogenitor cells, when treated with Insulin, mimic the process of chondrocyte differentiation (Atsumi et al., 1990; Shukunami et al., 1996). By immunostaining, we observed that following SCFD1, TANGO1 or STX18 knockdown *via* shRNA, Procollagen II formed large intracellular aggregates in greater than 60% of cells compared to 3% of cells in control samples (Fig. 5A–C). Q-PCR results also revealed, following SCFD1, TANGO1 or STX18 knockdown, that Col2 expression could not be maintained (Fig. S7A). To examine whether SCFD1 is generally involved in protein secretion in ATCD5 cell, metabolic labeling was applied. We found the overall pattern of secreted proteins detected by SDS-PAGE was not affected by SCFD1, TANGO or STX18 knockdown (Fig. S7B), which was consistent with previous observations in other cell lines (Nogueira et al., 2014). By using Alcian blue staining, we also found that compared to control cultures, knockdown of SCFD1, TANGO1 or STX18 all resulted in markedly reduced formation of cartilage-like matrix (Fig. S7C–G). Further experiments confirmed knockdown of SCFD1, TANGO1 or STX18 activated UPR and led to extensive apoptosis in ATCD5 cells (Fig. 5D and E). Together, these data suggest that SCFD1 and STX18 play a conserved and central role in Collagen II transport during chondrogenesis.

4. Summary

Here we report *in vivo* functional analysis of the Sec1/Munc18 family member SCFD1. Our experiments indicate that during chondrocyte differentiation SCFD1, acting with TANGO1 and STX18, is an indispensable factor for assembling mega-carriers to transport Collagen II from the ER to Golgi body. Loss of Scfd1 in zebrafish leads to intracellular protein buildup and activates the unfolded protein response in chondrocytes, leading to chondrocyte apoptosis and improper jaw cartilage formation. This work provides insight into function of SCFD1 in vertebrate development, and suggests a possible role for SCFD1 and its interacting partner proteins in craniofacial and other skeletal diseases.

Ethics approval

Zebrafish were housed and handled as per Canadian Council on Animal Care and Hospital for Sick Children Laboratory Animal Services guidelines. All the protocols involving the use of animals were in accordance with approved guidelines of the Institutional Animal Care and Use Committee of the Nanjing University.

Competing interests

The authors declare no competing financial interests.

Author contributions

X.L. and I.C.S. conceived and supervised the project and wrote the manuscript. N.H., Y.Y., and X.L. performed all experiments.

Funding

This research was undertaken, in part, thanks to the grant funding from the Natural Sciences and Engineering Research Council of Canada (RGPIN 341545 to I.C.S.) and National Natural Science Foundation of China (NSFC 31671505 and NSFC 31471354 to X.L).

Acknowledgements

We thank Stephen C. Ekker for the kind gift of GBT-RP2 gene trap plasmid, Thomas F. Schilling for the kind gift of *Tg(sox10:eGFP)* ^{ir937} zebrafish, Huajian Teng for the kind gift of ATDC5 cell line, Xiaoqin Wang for zebrafish husbandry and members of the Scott lab at the Hospital for Sick Children, Qi Xiao and Di Chen at Nanjing University for feedback and help during this project.

Appendix A. Supporting information

Supplementary data associated with this article can be found in the online version at doi:10.1016/j.ydbio.2016.11.010.

References

Atsumi, T., Miwa, Y., Kimata, K., Ikawa, Y., 1990. A chondrogenic cell line derived from a differentiating culture of AT805 teratocarcinoma cells. Cell Differ. Dev. 30, 109–116.
Bateman, J.F., Boot-Handford, R.P., Lamande, S.R., 2009. Genetic diseases of connective tissues: cellular and extracellular effects of ECM mutations. Nat. Rev. Genet 10, 173–183.
Burrows, J.T., Pearson, B.J., Scott, I.C., 2015. An in vivo requirement for the mediator subunit med14 in the maintenance of stem cell populations. Stem Cell Rep. 4, 670–684.
Caron, S.J., Prober, D., Choy, M., Schier, A.F., 2008. In vivo birthdating by BAPTISM reveals that trigeminal sensory neuron diversity depends on early neurogenesis. Development 135, 3259–3269.
Carr, C.M., Rizo, J., 2010. At the junction of SNARE and SM protein function. Curr. Opin. Cell Biol. 22, 488–495.
Clark, K.J., Balciunas, D., Pogoda, H.M., Ding, Y., Westcot, S.E., Bedell, V.M., Greenwood, T.M., Urban, M.D., Skuster, K.J., Petzold, A.M., Ni, J., Nielsen, A.L., Patowary, A., Scaria, V., Sivasubbu, S., Xu, X., Hammerschmidt, M., Ekker, S.C., 2011. In vivo protein trapping produces a functional expression codex of the vertebrate proteome. Nat. Methods 8, 506–515.
Dascher, C., Balch, W.E., 1996. Mammalian Sly1 regulates syntaxin 5 function in endoplasmic reticulum to Golgi transport. J. Biol. Chem. 271, 15866–15869.
DeLise, A.M., Fischer, L., Tuan, R.S., 2000. Cellular interactions and signaling in cartilage development. Osteoarthr. Cartil. 8, 309–334.
Fribley, A., Zhang, K., Kaufman, R.J., 2009. Regulation of apoptosis by the unfolded protein response. Methods Mol. Biol. 559, 191–204.
Goldring, M.B., Tsuchimochi, K., Ijiri, K., 2006. The control of chondrogenesis. J. Cell Biochem. 97, 33–44.
Hetz, C., 2012. The unfolded protein response: controlling cell fate decisions under ER stress and beyond. Nat. Rev. Mol. Cell Biol. 13, 89–102.
Lamande, S.R., Bateman, J.F., 1999. Procollagen folding and assembly: the role of endoplasmic reticulum enzymes and molecular chaperones. Semin. Cell Dev. Biol. 10, 455–464.
Laufman, O., Kedan, A., Hong, W., Lev, S., 2009. Direct interaction between the COG complex and the SM protein, Sly1, is required for Golgi SNARE pairing. EMBO J. 28, 2006–2017.
Li, Y., Gallwitz, D., Peng, R., 2005. Structure-based functional analysis reveals a role for the SM protein Sly1p in retrograde transport to the endoplasmic reticulum. Mol. Biol. Cell 16, 3951–3962.
Lobingier, B.T., Nickerson, D.P., Lo, S.Y., Merz, A.J., 2014. SM proteins Sly1 and Vps33 co-assemble with Sec17 and SNARE complexes to oppose SNARE disassembly by Sec18. eLife 3, e02272.
Melville, D.B., Montero-Balaguer, M., Levic, D.S., Bradley, K., Smith, J.R., Hatzopoulos, A.K., Knapik, E.W., 2011. The feelgood mutation in zebrafish dysregulates COPII-dependent secretion of select extracellular matrix proteins in skeletal morphogenesis. Dis. Models Mech. 4, 763–776.
Minoux, M., Rijli, F.M., 2010. Molecular mechanisms of cranial neural crest cell migration and patterning in craniofacial development. Development 137, 2605–2621.
Mow, V.C., Ratcliffe, A., Poole, A.R., 1992. Cartilage and diarthrodial joints as paradigms for hierarchical materials and structures. Biomaterials 13, 67–97.
Nechiporuk, A., Poss, K.D., Johnson, S.L., Keating, M.T., 2003. Positional cloning of a temperature-sensitive mutant emmental reveals a role for sly1 during cell proliferation in zebrafish fin regeneration. Dev. Biol. 258, 291–306.
Nogueira, C., Erlmann, P., Villeneuve, J., Santos, A.J., Martinez-Alonso, E., Martinez-Menarguez, J.A., Malhotra, V., 2014. SLY1 and Syntaxin 18 specify a distinct pathway for procollagen VII export from the endoplasmic reticulum. eLife 3, e02784.
Piloto, S., Schilling, T.F., 2010. Ovo1 links Wnt signaling with N-cadherin localization during neural crest migration. Development 137, 1981–1990.
Rauch, F., Glorieux, F.H., 2004. Osteogenesis imperfecta. Lancet 363, 1377–1385.
Rowe, T., Dascher, C., Bannykh, S., Plutner, H., Balch, W.E., 1998. Role of vesicle-associated syntaxin 5 in the assembly of pre-Golgi intermediates. Science 279, 696–700.
Sarmah, S., Barrallo-Gimeno, A., Melville, D.B., Topczewski, J., Solnica-Krezel, L., Knapik, E.W., 2010. Sec24D-dependent transport of extracellular matrix proteins is required for zebrafish skeletal morphogenesis. PLoS One 5, e10367.
Sasaki, M.M., Nichols, J.T., Kimmel, C.B., 2013. edn1 and hand2 interact in early regulation of pharyngeal arch outgrowth during zebrafish development. PLoS One 8, e67522.
Shukunami, C., Shigeno, C., Atsumi, T., Ishizeki, K., Suzuki, F., Hiraki, Y., 1996. Chondrogenic differentiation of clonal mouse embryonic cell line ATDC5 in vitro: differentiation-dependent gene expression of parathyroid hormone (PTH)/PTH-related peptide receptor. J. Cell Biol. 133, 457–468.
Sophia Fox, A.J., Bedi, A., Rodeo, S.A., 2009. The basic science of articular cartilage: structure, composition, and function. Sports Health 1, 461–468.
Steegmaier, M., Oorschot, V., Klumperman, J., Scheller, R.H., 2000. Syntaxin 17 is abundant in steroidogenic cells and implicated in smooth endoplasmic reticulum membrane dynamics. Mol. Biol. Cell 11, 2719–2731.
Stuhlmiller, T.J., Garcia-Castro, M.I., 2012. Current perspectives of the signaling pathways directing neural crest induction. Cell Mol. Life Sci. 69, 3715–3737.
Thisse, C., Thisse, B., 2008. High-resolution in situ hybridization to whole-mount zebrafish embryos. Nat. Protoc. 3, 59–69.
Vandewynckel, Y.P., Laukens, D., Geerts, A., Bogaerts, E., Paridaens, A., Verhelst, X., Janssens, S., Heindryckx, F., Van Vlierberghe, H., 2013. The paradox of the unfolded protein response in cancer. Anticancer Res. 33, 4683–4694.
Verduzco, D., Amatruda, J.F., 2011. Analysis of cell proliferation, senescence, and cell death in zebrafish embryos. Methods Cell Biol. 101, 19–38.
Walker, M.B., Kimmel, C.B., 2007. A two-color acid-free cartilage and bone stain for zebrafish larvae. Biotech. Histochem. 82, 23–28.
Wang, M., Kaufman, R.J., 2014. The impact of the endoplasmic reticulum protein-folding environment on cancer development. Nat. Rev. Cancer 14, 581–597.
Westerfield, M., 1993. The Zebrafish book: a guide for the laboratory use of Zebrafish Danio (Brachydanio) rerio. University of Oregon Press, Oregon.
Yamaguchi, T., Dulubova, I., Min, S.W., Chen, X., Rizo, J., Sudhof, T.C., 2002. Sly1 binds to Golgi and ER syntaxins via a conserved N-terminal peptide motif. Dev. Cell 2, 295–305.
Yan, Y.L., Miller, C.T., Nissen, R.M., Singer, A., Liu, D., Kirn, A., Draper, B., Willoughby, J., Morcos, P.A., Amsterdam, A., Chung, B.C., Westerfield, M., Haffter, P., Hopkins, N., Kimmel, C., Postlethwait, J.H., 2002. A zebrafish sox9 gene required for cartilage morphogenesis. Development 129, 5065–5079.
Yang, L., Ma, X., Lyone, A., Zou, J., Blackburn, M.L., Pan, J., Yang, D., Matsushita, H., Mei, B., Zielinska-Kwiatkowska, A., Chansky, H.A., 2009. Proper expression of helix-loop-helix protein Id2 is important to chondrogenic differentiation of ATDC5 cells. Biochem. J. 419, 635–643.
Zuscik, M.J., Hilton, M.J., Zhang, X., Chen, D., O'Keefe, R.J., 2008. Regulation of chondrogenesis and chondrocyte differentiation by stress. J. Clin. Investig. 118, 429–438.